Bulletin of the Seismological Society of America, Vol. 89, No. 1, pp. 317–324, February 1999

Basin Waves on a Seafloor Recording of the 1990 Upland, California, Earthquake: Implications for Ground Motions from a Larger Earthquake

by David M. Boore

Abstract The velocity and displacement time series from a recording on the seafloor at 74 km from the 1990 Upland earthquake (**M** = 5.6) are dominated by late-arriving waves with periods of 6 to 7 sec. These waves are probably surface waves traveling across the Los Angeles basin. Response spectra for the recording are in agreement with predictions from empirical regression equations and theoretical models for periods less than about 1 sec but are significantly larger than those predictions for longer periods. The longer-period spectral amplitudes are controlled by the late-arriving waves, which are not included in the theoretical models and are underrepresented in the data used in the empirical analyses. When the motions are scaled to larger magnitude, the results are in general agreement with simulations of wave propagation in the Los Angeles basin by Graves (1998).

Introduction

For more than 20 years, digitally recording triggered accelerometers have been installed on the seafloor near some of the oil platforms off of the southern California coast. These instruments, installed by the Seafloor Earthquake Measuring System (SEMS) project, are designed to obtain ground shaking data on the seafloor that can be used to evaluate the design of offshore oil platforms. Boore and Smith (1999) and Boore (1997) contain an analysis of the largest earthquakes recorded through 1997 on this system. Those studies, however, limit the analysis to the ground motion carried in the *S*-wave portion of the time series. This was done because not all of the records were of sufficient duration to capture later arriving waves. One recording, of the 1990 Upland earthquake (**M** = 5.6), did include these later arriving waves and showed that the peak velocity and peak displacement of the ground motion were carried by these later waves. The waves traversed the Los Angeles basin for most of their travel path and are probably an excellent example of what are often called *basin waves*—surface waves converted from body waves at the edge of a basin and traveling at much slower group velocities than the body waves (e.g., Hanks, 1975; Vidale and Helmberger, 1988; Joyner, 1998). I show that the response spectra due to these basin waves can be a factor of 5 to more than 10 times larger than expected from standard predictions of ground motions. I also use the recording of the **M** 5.6 earthquake to predict the motions that would have been observed for the same source and receiver location from a **M** 7.5 earthquake. The results suggest that the basin waves will be of predominate importance for the response of structures with resonant periods greater than a few seconds.

Basin Waves on the Recording

The location of the epicenter (UP90) and recording station (S3E) are shown in Figure 1. The sensor (a force-balance accelerometer) is buried 1.5 m beneath the seafloor, and the water depth is 64 m. Boore and Smith (1999) conclude that the water will have almost no influence on the horizontal components of earthquake-induced ground shaking for frequencies of engineering interest. Most of the path along the surface from the epicenter to the station is in the Los Angeles basin (Yerkes *et al.*, 1965; station S3E is just northeast of the Palos Verdes fault, which lies within the basin), and the path is more or less perpendicular to the axis of the basin. This makes the record useful as a check of numerical simulations of wave propagation in basins [such as those of Olsen *et al.* (1995) and Graves (1998)], particularly because the source duration should be much less than the dominant period of ground displacements, and therefore, complexities in the record are more likely to be related to travel path than to the source.

The recorded acceleration time series, and the velocity and displacement time series obtained from integration of the acceleration records, are displayed in Figure 2. (Absolute orientations are not available for station S3E, and therefore, the two horizontal components are referred to simply as "x" and "y".) Figure 2a gives the three components of acceleration plotted to a common scale and shows that the vertical accelerations are much smaller than the horizontal accelerations. This is a common feature in seafloor ground motions, which Boore and Smith (1999) attribute to the soft sediments under the site as well as to effects of the water layer. Figures 2b, 2c, and 2d show the three measures of ground shaking

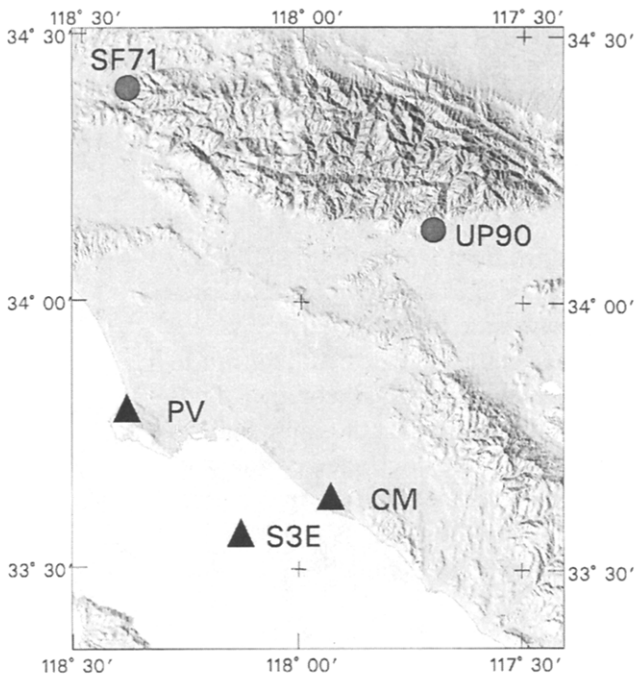

Figure 1. Map of portion of southern California, showing the epicenters of the 1971 San Fernando (SF71) and 1990 Upland (UP90) earthquakes, as well as the stations providing data used in this article. SF71 was recorded on stations CM and PV, while UP90 was recorded on station S3E (station S3E is the same as station S3EE in Boore and Smith, 1999). The paths from SF71 to CM and PV are almost entirely within the Los Angeles basin, as is the path from UP90 to S3E (the basin boundary lies to the southwest of station S3E).

plotted with individual normalization. Both the peak velocities and peak displacements occur well after the peak acceleration, and the peak displacements are carried by waves with periods around 6 sec.

The recorder had a pre-event buffer, and the relatively small oscillations in the displacement traces prior to the *P*-wave arrival is a strong indication that the signal is significantly above long-period recorder or microseism noise.

The ground motions for one of the horizontal components ("x") are compared in Figure 3 with the horizontal components of the 1971 San Fernando earthquake (**M** = 6.6) recorded at stations CM and PV. As with the recording at S3E, the horizontal wave path to CM and PV traverses the Los Angeles basin, although through a different part of the basin (Fig. 1). There is a striking qualitative similarity between the much smaller recordings of the 1990 Upland earthquake and those from the 1971 San Fernando earthquake. The enhanced long-period motion of the basin waves relative to the body-wave arrivals shown in Figure 3c is probably due to several effects: the long resonant period of the wave guide formed by the deep basin, the much smaller geometrical spreading for the surface waves than for the body waves, and the loss of high-frequency motion to scattering and intrinsic attenuation while the surface waves traverse the basin.

To make a quantitative estimate of the importance of these basin waves for the amplitude of ground shaking, the response spectrum for the complete record are compared with the following "standard" estimates of response spectra in Figure 4: (1) empirical regression equations published by Abrahamson and Silva (1997) and Boore *et al.* (1997) and (2) simulations of the ground motions using the stochastic model (e.g., Boore, 1997).

The empirical regression analyses were evaluated for a soil whose average velocity to 30 m depth equals that estimated for station S3E (216 m/sec; see Boore and Smith, 1999); this required an adjustment for the Abrahamson and Silva equations, which are for soil, by using Boore *et al.*'s (1997) factors to go from 310 m/sec (an average soil) to 216 m/sec (the period-dependent adjustment factor is at most 1.26). Because of limited recording durations or length of analog records actually digitized, the filtering of long-period motions, and the inclusion of nonbasin stations, the empirically based long-period analyses almost certainly underestimate the contribution from basin waves (long period in an engineering context is generally between about 2 and 10 sec). Abrahamson and Silva (1997) made a special effort to extract long-period signals from analog strong-motion recordings, and therefore, their equations probably contain a greater contribution from the basin waves than do the equations of Boore *et al.* (1997).

The stochastic model simulations used the source model of Atkinson and Boore (1998), site amplifications given by quarter-wavelength amplifications (e.g., Boore and Brown, 1998) applied to the velocity profile estimated for the S3E site (given in Boore and Smith, 1999) and other parameters as given in Table 1. The stochastic model assumes that the motion is made up of body waves, with no special allowance for basin waves.

It is clear from Figure 4 that the standard methods for estimating ground motion underestimate the long-period motions, by factors ranging from about 5 to over 10 at the period of peak response.

As an additional way of indicating the importance of basin waves, the response spectrum computed from only the *S*-wave portion of the S3E record is also shown in Figure 4. The response spectrum near 7-sec period without the basin waves is more than a factor of 10 times smaller than with the basin waves, again emphasizing the importance of the basin waves at long periods.

The good comparison of the stochastic model simulation to the empirical results for periods less than 1.0 and to the response spectra computed from the body-wave portion of the record at long periods suggests that the stochastic model can be used to extrapolate the empirical results to long periods for cases in which no basin waves are present (the underprediction of the stochastic model results compared with those of Abrahamson and Silva at periods greater than 1 sec may be due to the presence of basin waves in some of the data used in developing their empirical attenuation equations).

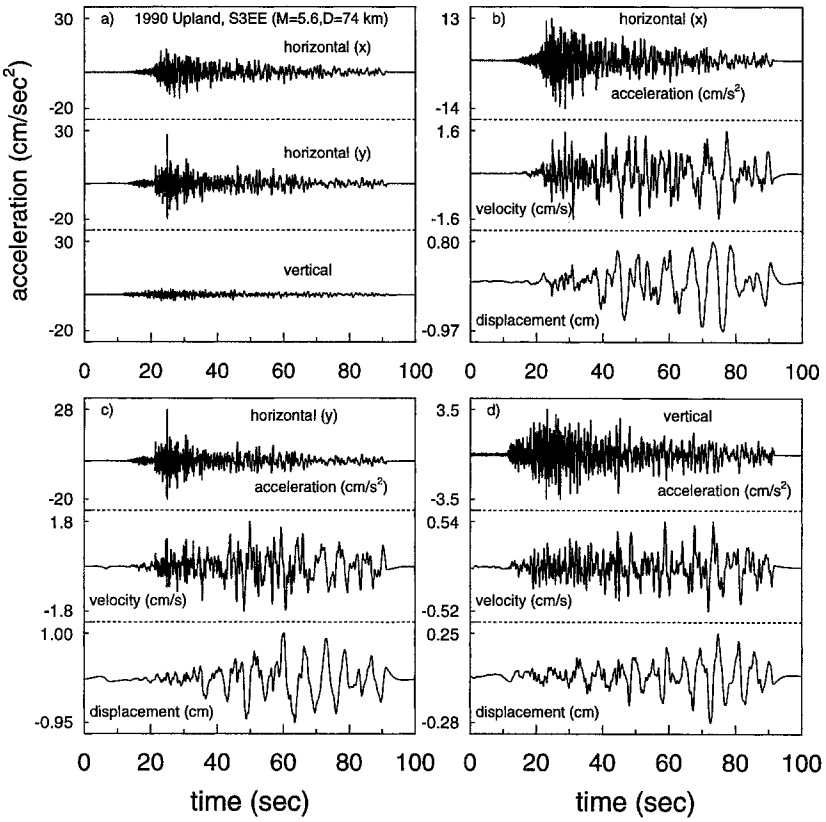

Figure 2. (a) Three-component accelerograms, in cm/sec^2, of the Upland 1990 earthquake recorded at station S3E, plotted using the same vertical scale to emphasize the relative amplitude of the components. (b), (c), and (d) Acceleration (cm/sec^2), velocity (cm/sec), and displacement (cm) time series for the three components of the S3E recording of the 1990 Upland earthquake, plotted using different vertical scales, to emphasize the appearance of the waveforms. Note the dominance of late-arriving 5- to 7-sec waves on the displacement trace, something not emphasized in the accelerogram.

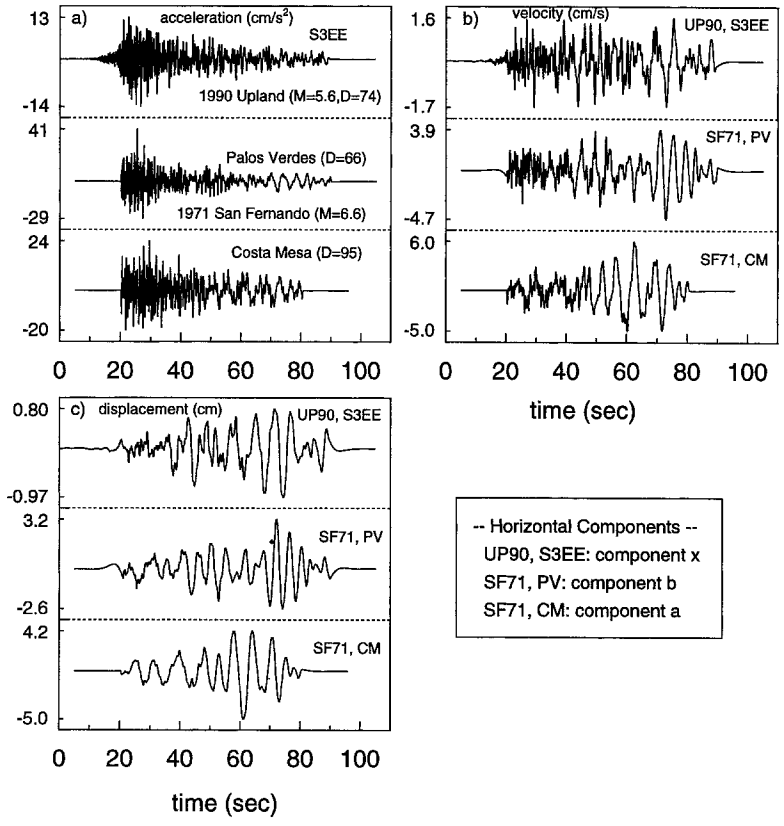

Figure 3. Horizontal-component accelerations (cm/sec^2), velocities (cm/sec), and displacements (cm) from the 1990 Upland earthquake recorded offshore at S3E (*top trace*) and from the larger 1971 San Fernando earthquake recorded at Palos Verdes and Costa Mesa (*middle* and *bottom traces,* respectively). The accelerograms were low-cut filtered at 0.1 Hz before integration to velocity and displacement. The two 1971 recordings apparently triggered on the *S* wave, but it is unlikely that the response spectra at the longer periods will be affected by the short duration of missing *S* energy. The durations of the accelerograms represent the complete recording, after which the triggered instruments turned off. It is likely that the long-period energy continued for a longer duration. Note the overall similarity in the waveforms, despite the factor of up to 5 disparity in peak amplitudes.

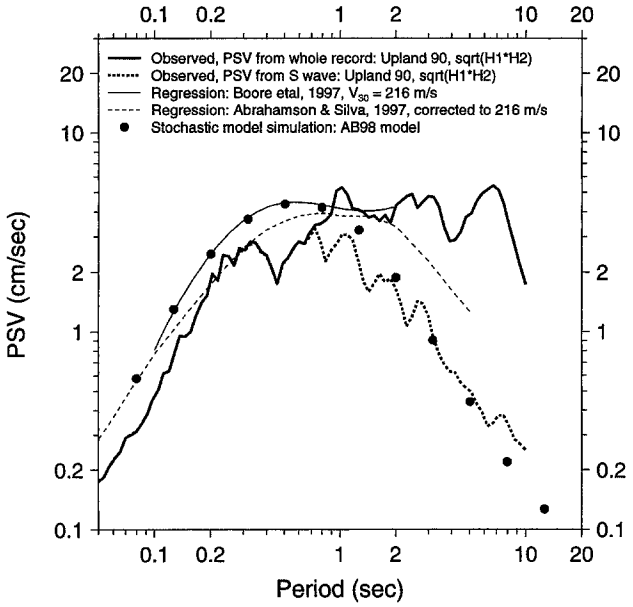

Figure 4. Observed and predicted 5%-damped pseudo-relative velocity response spectra (PSV) for the horizontal components of motion at station S3E from the 1990 Upland earthquake. The heavy lines are from the observed data: the solid and dashed lines being the PSV from the whole record and from the *S*-wave portion of the record (the first 35 sec of record shown in Fig. 2), respectively. The spectra are the geometric mean of the spectra for the two horizontal components. The light lines are from empirical regression equations published by Abrahamson and Silva (1997) and Boore *et al.* (1997), and the dots are theoretical predictions assuming body-wave arrivals and the source model of Atkinson and Boore (1998) (AB98).

Scaling the Motions to Those from an **M** = 7.5 Earthquake

This section explores scaling up the S3E record to give the ground motions from a larger earthquake (**M** = 7.5 in this application). The scaling must account for differences in source spectra and differences in duration of shaking. The algorithm for doing the scaling follows:

- Construct a duration filter by filling an array whose duration equals the difference in source duration of the large and small earthquakes with Gaussian random numbers, normalized so that the amplitude spectrum has unit squared amplitude when averaged over frequency.
- Multiply the spectrum of the duration filter by the theoretical ratio of source spectra for the large earthquake and an earthquake with a magnitude equal to that of the small earthquake.
- Multiply the product of the above by the spectrum of the small earthquake.
- Inverse transform to obtain the time series of the large event.
- Compute velocity, displacement, and response spectra from the resulting acceleration time series.

Table 1

Parameters of the stochastic models. Unless noted, the parameters were used for both the AB98 and B70 models.

Source Properties
• Material properties: ρ = 2.7 gm/cm^3, β = 3.7 km/sec
• Radiation coefficient = 0.55
• AB98 model: as given by the AB98-Ca model in Tables 4 and 5 of Atkinson and Boore (1998)
• B70 model: single-corner frequency, ω^{-2}, with $\Delta\sigma$ = 70 bars
Path Properties
• Whole-path attenuation: $Q = 204(f/1.0)^{0.56}$
• Geometrical spreading: r^{-1} to 50 km, r^0, from 50 to 170 km, $r^{-0.5}$ beyond 170 km.
• Duration = $1/f_0 + 0.05r$, where f_0 is the low-frequency corner.
Site Properties
• Partition factor = 0.707
• Free-surface factor = 2.0
• Diminution factor: AB98: $\kappa = 0.0516 + 0.0106\,(\mathbf{M} - 6)$; B70: $\kappa = 0.058$
• Site amplification, relative to the source depth, represented by straight lines in log frequency, log amplification space, connecting the following points (see Boore, 1996, for details of usage):

Frequency	Amplification
0.010	1.00
0.038	1.09
0.071	1.21
0.13	1.48
0.34	2.48
0.64	3.99
4.26	5.76

Several assumptions are made in this method: (1) the materials remain linear, even for strong shaking, (2) all of the path effects are captured by the small event (this might not be true for an extended rupture, for which energy for different parts of the rupture would not be traveling along the same path), and (3) the magnitude scaling of the spectra for the basin waves is the same as for the source spectra. I discuss the assumption of linearity later. The validity of the second assumption is hard to assess, but the strike of one of the conjugate fault planes for the Upland earthquake (306°, Dreger and Helmberger, 1991) is approximately perpendicular to the azimuth from the source to station S3EE (212°). In the method used here, the larger earthquake has the same focal mechanism as the smaller event, and if we assume that rupture is elongated on the fault plane striking 306°, the source-to-station distances will be approximately the same for much of the rupture in the larger earthquake. The third assumption is justified assuming linearity and the formation of basin waves from the conversion of body waves at the basin edge.

I used two source models in this application: (1) the regression-based source model of Atkinson and Boore (1998), and (2) the single-corner-frequency, constant-stress-drop Brune (1970, 1971) source; these are hereafter referred to as "AB98" and "B70". The AB98 model is a modified

version of the Atkinson and Silva (1997) model, which is based on fitting Fourier amplitude spectra from strong-motion recordings of California earthquakes. The AB98 model has two corner frequencies and a high-frequency spectral level that scales less rapidly with magnitude than given by a constant stress drop model (such as the B70 model). In addition, the high-frequency diminution parameter κ in the AB98 model is not constant but depends on magnitude as given in Table 1. The ground-motion spectra for the AB98 and the B70 models are shown in Figure 5. For both models, the magnitude scaling at long periods is greater than at short periods. This controls the enrichment of long-period energy in larger earthquakes. The AB98 model gives a spectrum for the large earthquake that is about a factor of 3 smaller at long periods than the spectrum from the B70 model. At short periods, the magnitude scaling is smaller for the AB98 model than for the B70 model. All of these features will show up in the simulated time series and response spectra.

The acceleration time series that results from scaling the observed motion at S3E for the **M** = 5.6 Upland earthquake to what would have been observed at the same site and the same distance for an **M** = 7.5 earthquake are shown in Figure 6a. The velocity and displacement time series obtained from the acceleration traces are shown in Figures 6b and 6c. In each figure, the motion for the smaller earthquake is given at the bottom and the scaled-up motions for the two source scalings are given in the upper two traces. Note the large long-period motions late in the scaled-up motions. For the **M** = 7.5 earthquake, this long-period motion is stronger relative to the short-period motion at the beginning of the traces than it is for the **M** = 5.6 earthquake; this is a consequence of the shift in corner frequencies to lower frequency as the moment increases. The difference is less pronounced for the AB98 model; this is a result of the "sag" in their spectra relative to the single-corner-frequency B70 spectra (Fig. 5).

The predicted velocity and displacements are very large, particularly for the B70 model (but not larger than recorded elsewhere in other earthquakes). Is it possible that the assumption of linearity is violated by such large motions? The critical factor in assessing this is the strain induced by the waves in the ground. The strains in the surface waves can be approximated by the ratio of ground velocity to propagation velocity (e.g., Spudich *et al.*, 1995). The propagation velocity for the basin waves is at least 1 km/sec (Joyner, 1997), giving strains less than 0.001. Standard modulus degradation and damping curves used in engineering analysis of soil (e.g., chap. 6 in Kramer, 1996) indicate that some nonlinear response is expected for strains of 0.001, but these curves are for soils at shallow depths (less than 100 m). Most of the energy in the surface waves is transmitted at significantly greater depths. The materials at these depths are much stronger than the soils for which the modulus reduction and damping curves apply, and therefore, nonlinearity will be substantially smaller. How much smaller is unknown, in the absence of laboratory or *in situ* measurements of the nonlinear response.

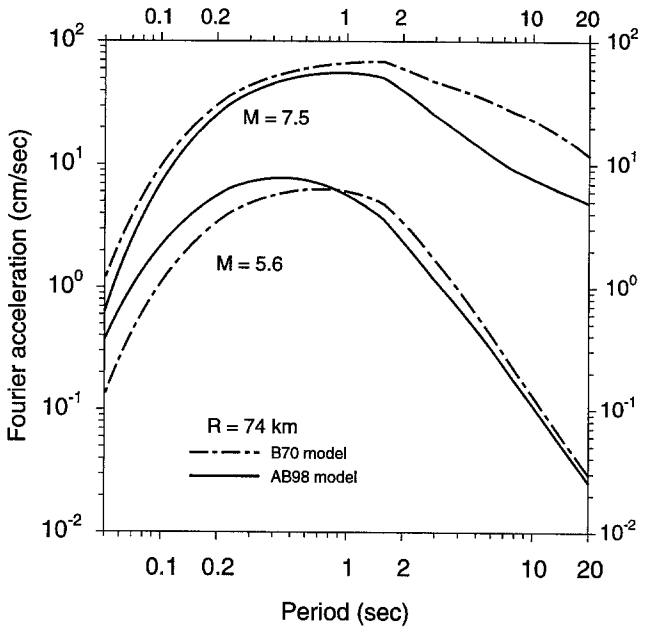

Figure 5. Fourier amplitude spectra at a distance of 74 km for the two source models and the two magnitudes considered in this article. [AB98 is Atkinson and Boore (1998) and B70 is Brune (1970, 1971).] The model parameters used in the calculations are given in Table 1. For ease of comparison with other figures in this article, the abscissa is in units of period rather than frequency. Note the much larger difference in amplitudes at long periods than at short periods, a feature found in most, if not all, source models.

A useful measure of the characteristics of the motions is given by their response spectra, shown in Figure 7 for the AB98 model and Figure 8 for the B70 model. The comparisons in these figures tell a number of things (some of which were commented on in discussing Fig. 4). Note first the relatively good agreement between the response spectra from the S3E recording on the ocean floor and the regression-based results for periods from about 0.2 to 2 sec. This suggests that the horizontal-component S3E motions are not strongly influenced by the presence of the water layer. The next thing to note is the good comparison between the simulated and regression-based motions for periods up to about 1 sec, particularly for the AB98 model. Focusing on the long periods, the large mismatch for **M** = 5.6 between the observed motion and the predicted motions at long periods carries over to the motions for the **M** = 7.5 earthquake and, combined with the source scaling, produces the large motions for that earthquake at long periods. The mismatch is a result of the presence of basin waves on the S3E record for the smaller earthquake. Finally, comparing Figures 7 and 8 indicates that although both the AB98 and B70 source models predict motions in relatively good agreement with the regression-based results for the smaller earthquake for periods less than about 1.0 sec, the AB98 model is in better agreement with the regression-based results for the larger earthquake.

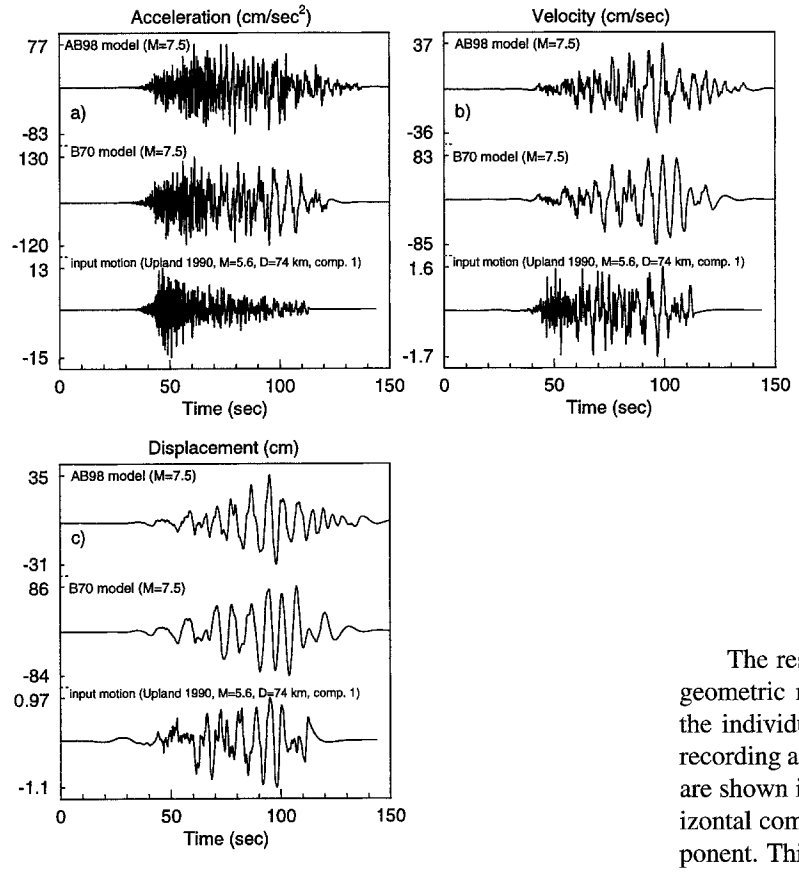

Figure 6. The simulated time series for an **M** = 7.5 earthquake, derived by scaling the S3E recording of the **M** = 5.6 1990 Upland earthquake (*bottom trace*) using the Atkinson and Boore (1998) (AB98) and Brune (1970, 1971) (B70) source models. The velocity and displacement traces in panels (b) and (c) were derived by integrating the acceleration time series in panel (a), after applying a low-cut filter between 0.05 and 0.1 Hz. The bottom trace is the recorded motion, and upper two traces are the motions for the larger earthquake, based on the indicated source models.

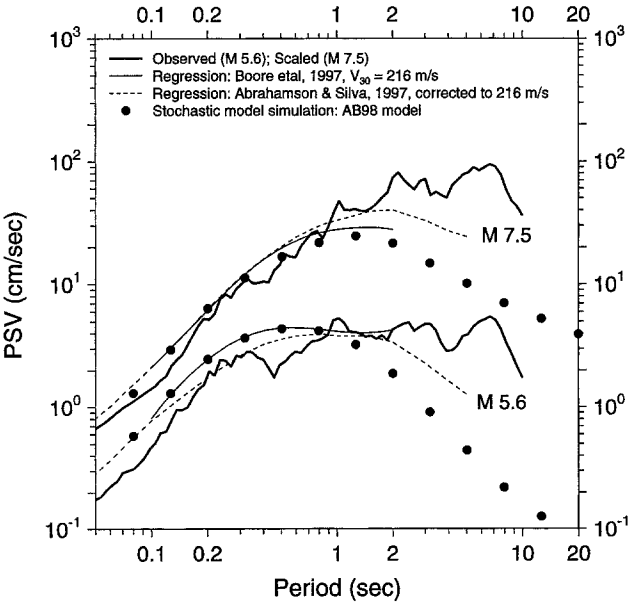

Figure 7. 5%-damped, pseudo-velocity response spectra (PSV) for the small earthquake (**M** = 5.6) and the large earthquake (**M** = 7.5) (heavy solid lines). The PSV for the large event has been derived from the small event assuming Atkinson and Boore (1998) (AB98) source models. Also shown are the predictions from two regression analyses (light solid and dashed lines) and from stochastic-model simulations (solid circles).

The response spectra shown in Figures 7 and 8 are the geometric means of the individual horizontal components; the individual spectra and the means for the 1990 Upland recording and the scaled-up motions, using the AB98 model, are shown in Figure 9, which shows that the individual horizontal components are similar to the mean horizontal component. This is not to say that rotating the two components into radial and transverse components would not reveal physically significant differences in the ground motions. I could not rotate the components because the component azimuths were not available for the S3E recording. Even if they were, lateral refraction over long travel paths can introduce *P* and *SV* motion onto the transverse component, and vice versa, and the regression results and stochastic model simulations are in terms of the random horizontal component, which is given by the geometric mean of the two horizontal components.

Graves (1998) includes simulations for a site (FTNV) in the Los Angeles basin for a source on the San Andreas fault, outside of the basin. Coincidentally, the distance from the source to the station (74 km) and the magnitude of the earthquake (**M** = 7.5) are the same as in my scaling. His motions have a similar duration to those in Figure 6, but comparisons of peak motions is complicated by the different periods of the dominant motions in his simulated time series (around 3 sec compared with 6 sec in Fig. 6) and the different velocity models in the two simulations. His model is capped at a lower shear-wave velocity of 1.0 km/sec, whereas the shear-wave velocities at the S3E site are certainly much lower than that. The difference in dominant period makes it difficult to compare peak velocities or displacements. He, however, gives predicted values for response spectra at a period of 4 sec. Based on calculations for appropriate velocity models, I estimate that the amplifications for the two velocity models differ by a factor of about 1.4 at a period of 4 sec. Applying this factor to the values in Table 7 of Graves (1998) gives amplitudes of 105 and 80 cm/sec for two slip time functions,

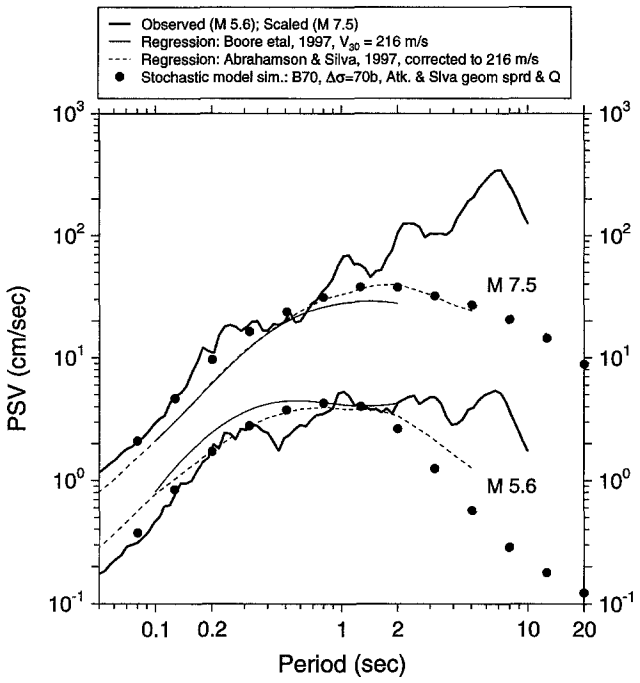

Figure 8. 5%-damped, pseudo-velocity response spectra (PSV) for the small earthquake (**M** = 5.6) and the large earthquake (**M** = 7.5) (heavy solid lines). The PSV for the large event has been derived from the small event assuming single-corner-frequency source model (B70) with a stress parameter of 70 bars. Also shown are the predictions from two regression analyses (light solid and dashed lines) and from stochastic-model simulations (solid circles).

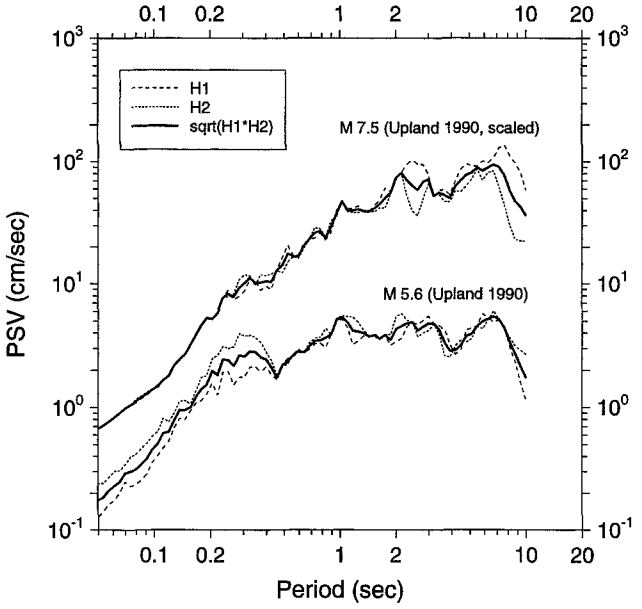

Figure 9. This figure demonstrates the insensitivity of the scaled results to the component of horizontal motion. As in Figure 7, the PSV for the large event has been derived from the small event assuming the Atkinson and Boore (1998) (AB98) model. The solid line is the geometric mean of the two horizontal components, shown by the dashed lines.

which he calls the filtered impulse and 2 sec CSTF slip time functions, respectively. Graves prefers the latter slip function, the response spectrum for which (80 cm/sec) compares well with the value of about 70 cm/sec in the vicinity of 4-sec period for the AB98 model in Figure 7.

Discussion and Conclusions

A particularly useful recording for the study of long-period motions in sedimentary basins was made at a site offshore of Long Beach at 74 km from the **M** = 5.6 1990 Upland earthquake. Much of the travel path was across the Los Angeles basin. Comparisons of response spectra from this recording with regression-based spectra and theoretical calculations, as well as time-domain comparisons with recordings from the 1971 San Fernando earthquake that have traveled through the Los Angeles basin, show that late-arriving, large-amplitude, long-period surface waves (basin waves) carry most of the ground motion at long periods and that standard predictions fall short of predicting the levels of ground shaking by substantial amounts. Structures whose periods are long enough to be influenced by these long periods may be rare, but methods for predicting motions with periods longer than about 2 sec may have to be revised if the propagation path between source and receiver contains a substantial portion of a basin. Scaling of the record to the motions expected for an **M** = 7.5 event are a general agreement with the simulations of Graves (1998). Agreement of the scaled motions with empirical regression results for periods less than about 1 sec gives support to the source model of Atkinson and Boore (1998).

Acknowledgments

This work would not have been possible without the efforts of Charles Smith of the Minerals Management Service, who championed the development and deployment of the SEMS stations and provided funding for this study. I wish to thank Bill Joyner for encouragement and criticisms and Jim Gibbs and an anonymous referee for careful reviews of the manuscript. The strong-motion programs of the California Division of Mines and Geology and the U.S. Geological Survey provided accelerograms and borehole velocities.

References

Abrahamson, N. A. and W. J. Silva (1997). Empirical response spectral attenuation relations for shallow crustal earthquakes, *Seism. Res. Lett.* **68,** 94–127.

Atkinson, G. M. and D. M. Boore (1998). Evaluation of models for earthquake source spectra in eastern North America, *Bull. Seism. Soc. Am.* **88,** 917–934.

Atkinson, G. M. and W. Silva (1997). An empirical study of earthquake source spectra for California earthquakes, *Bull. Seism. Soc. Am.* **87,** 97–113.

Boore, D. M. (1996). SMSIM—Fortran programs for simulating ground motions from earthquakes: version 1.0, *U.S. Geol. Surv. Open-File Rept. 96-80-A and 96-80-B,* 73 pp.

Boore, D. M. (1997). Analysis of earthquake recordings obtained from the Seafloor Earthquake Measurement System (SEMS) instruments de-

ployed off the coast of southern California, *U.S. Geol. Surv. Open-File Rept. 97-733,* 242 pp.

Boore, D. M. and L. T. Brown (1998). Comparing shear-wave velocity profiles from inversion of surface-wave phase velocities with downhole measurements: systematic differences between the CXW method and downhole measurements at six USC strong-motion sites, *Seism. Res. Lett.* **69,** 222–229.

Boore, D. M. and C. E. Smith (1999). Analysis of earthquake recordings obtained from the Seafloor Earthquake Measurement System (SEMS) instruments deployed off the coast of southern California, *Bull. Seism. Soc. Am.* **89,** 260–274.

Boore, D. M., W. B. Joyner, and T. E. Fumal (1997). Equations for estimating horizontal response spectra and peak acceleration from western North American earthquakes: a summary of recent work, *Seism. Res. Lett.* **68,** 128–153.

Brune, J. N. (1970). Tectonic stress and the spectra of seismic shear waves from earthquakes, *J. Geophys. Res.* **75,** 4997–5009.

Brune, J. N. (1971). Correction, *J. Geophys. Res.* **76,** 5002.

Dreger, D. S. and D. V. Helmberger (1991). Complex faulting deduced from broadband modeling of the 28 February 1990 Upland earthquake (M_L = 5.2), *Bull. Seism. Soc. Am.* **81,** 1129–1144.

Graves, R. W. (1998). Three-dimensional finite-difference modeling of the San Andreas fault: Source parameterization and ground-motion levels, *Bull. Seism. Soc. Am.* **88,** 881–897.

Hanks, T. C. (1975). Strong ground motion of the San Fernando, California, earthquake: ground displacements, *Bull. Seism. Soc. Am.* **65,** 193–225.

Joyner, W. B. (1998). Strong ground motion from surface waves generated at the edge of deep sedimentary basins (abstract), *Seism. Res. Lett.* **69,** 153.

Kramer, S. L. (1996). *Geotechnical Earthquake Engineering,* Prentice Hall, Upper Saddle River, New Jersey, 653 pp.

Olsen, K. B., R. J. Archuleta, and J. R. Matarese (1995). Three-dimensional simulation of a magnitude 7.75 earthquake on the San Andreas fault, *Science* **270,** 1628–1632.

Spudich, P., L. K. Steck, M. Hellweg, J. B. Fletcher, and L. M. Baker (1995). Transient stresses at Parkfield, California, produced by the **M** 7.4 Landers earthquake of June 28, 1992: observations from the UPSAR dense seismographic array, *J. Geophys. Res.* **100,** 675–690.

Vidale, J. E. and D. V. Helmberger (1988). Elastic finite-difference modeling of the 1971 San Fernando, California earthquake, *Bull. Seism. Soc. Am.* **78,** 122–141.

Yerkes, R. F., T. H. McCulloh, J. E. Schoellhamer, and J. G. Vedder (1965). Geology of the Los Angeles basin, California—an introduction, *U.S. Geol. Surv. Profess. Pap. 420-A,* 57 pp.

U.S. Geological Survey
345 Middlefield Road
Menlo Park, California 94025
E-mail: dboore@isdmnl.wr.usgs.gov

Manuscript received 23 April 1998.